

Article

Epidermal Gland Inspired Self-Repairing Slippery Lubricant-Infused Porous Coatings with Durable Low Ice Adhesion

Tong Li, Yizhi Zhuo , Verner Håkonsen, Sigrid Rønneberg, Jianying He * and Zhiliang Zhang 

NTNU Nanomechanical Lab, Department of Structural Engineering, Norwegian University of Science and Technology (NTNU), 7491 Trondheim, Norway; tong.li@ntnu.no (T.L.); yizhi.zhuo@ntnu.no (Y.Z.); verner.hakonsen@ntnu.no (V.H.); sigrid.ronneberg@ntnu.no (S.R.)

* Correspondence: jianying.he@ntnu.no (J.H.); zhiliang.zhang@ntnu.no (Z.Z.)

Received: 12 August 2019; Accepted: 22 September 2019; Published: 24 September 2019



Abstract: The limited durability of slippery lubricant-infused porous surfaces (SLIPS) restricts their practical applications. Inspired by the epidermal glands of skins, we developed a facile approach to durable SLIPS with gland-like storage and release functions for icephobicity. By introducing a hybrid surfactant as a lubricant into the polydimethylsiloxane (PDMS) matrix, lubricant capsules were formed and mono-dispersed in the matrix, working as gland-like structures to release lubricant. The obtained SLIPS showed durable low ice adhesion strength and thermal durability simultaneously. In detail, the enhanced durability for icephobicity was demonstrated by 20 icing/deicing tests, in which the lubricant remains on the surface; the coatings showed negligible weight loss when stored at 100 °C for 60 h, displaying pronounced thermal durability of the slippery effect. Our current strategy sheds new light on a facile fabrication of mechanically and thermally durable SLIPS for icephobicity.

Keywords: icephobicity; durability; slippery surface; epidermal gland; self-repairing property

1. Introduction

Ice formation and accretion is a severe hazard for transportation and infrastructures, causing events such as the collapse of infrastructure and traffic accidents [1–4]. The current deicing methods, including heating, salting and mechanically removing ice, are either eco-unfriendly or energy-intensive [5–9]. Passive icephobic materials are then developed, as they can mitigate and even prevent ice accretion without energy input [10–13]. For example, the accreted ice on some passive surfaces with low ice adhesion can be removed under the action of the gravity of ice or by natural winds [3,7,11,14–16].

So far, intensive studies on passive icephobic materials have led to the discovery of various strategies, including superhydrophobic surfaces and lubricant-infused surfaces [7,16–21]. Although the superhydrophobic surfaces have been successfully utilized for delaying water droplet freezing time and/or reducing water droplet contact area [20,22–25], they display mechanical weakness and/or the interlocking effect in harsh humidity, owing to hierarchical surface structures [26,27]. Slippery lubricant-infused porous surfaces (SLIPS) have attracted great attention and have been widely developed for high-performance icephobic materials [28–30]. In detail, such surfaces have excess lubricant infused into their pores, resulting in the liquid layer on the top [22,30,31]. This liquid layer not only prevents the ice from mechanically interlocking with the solid substrate, but also displays high mobility, which makes the ice detach easily remove from the surfaces. However, the lubricant may evaporate from the surfaces and be quickly depleted in cycles of the mechanical deicing process [32,33], following a reduction in the icephobicity of the SLIPS. The ice adhesion strength may quickly increase

after only one icing/deicing cycle [2,32]. Hence, enhancing the durability is a key and urgent issue for the icephobic SLIPS.

Some strategies have been developed to increase the durability of SLIPS, including enhancement of physical interaction between the lubricant and the porous substrate, covalent immobilization of the lubricant and reduction of lubricant evaporation [34–37]. However, the durability of the SLIPS with low ice adhesion still needs to be studied further [29,37,38]. Recently, a concept was proposed for creating low ice adhesion surfaces with long-term infusion stability based on elasticity, superhydrophobicity and SLIPS [37]. Very recently, UV-cured siloxane resins in the porous anodic aluminum oxide structures, which are used to enhance the icephobic durability of the SLIPS surfaces, have been reported [32]. The ice adhesion was tested by removing the ice in a centrifuge at $-15\text{ }^{\circ}\text{C}$. After eight icing/deicing cycles, the ice adhesion strength of the SLIPS increased from about 8 to 50 kPa. The icephobic durability of the SLIPS still needs to be further improved. Frogs, earthworms and some fishes are known to have durably slippery skins because of their self-lubricating mechanism (Figure S1) [39–41]. Their epidermal glands can continuously secrete mucus and result in durable lubricating surfaces [42,43]. Sun et al. obtained the antifreeze-secreting coatings by spraying a hierarchical polymeric superhydrophobic shell onto a nylon membrane [43]. Another such self-secreting SLIPS was prepared by casting a mixture that consists of a copolymer of urea and polydimethylsiloxane, silicone oil and THF [41]. Alternatively, a sandwich SLIPS was introduced to enhance the surface stability, in which a middle lubricant layer could self-secrete lubricant to the surface once the surface lubricant layer was depleted [44]. These approaches to the secreting SLIPS need either multistep or extra organic solvent. Moreover, there are only a few studies about SLIPS with durable low ice adhesion strength through the self-secretion or resupply of the lubricant.

Herein, we imitated the functions of the epidermal glands and developed a facile approach to SLIPS coating with gland-like storage and release function for icephobicity. Hybrid surfactant was encapsulated into the polydimethylsiloxane (PDMS) matrix, working as a gland-like structure to release lubricant. The obtained coatings displayed a durable slippery effect that was derived from the self-releasing of the lubricant on the surfaces. The surface of the optimized coating still contained lubricant after 20 icing/deicing cycles, where the ice adhesion strength slightly increased from 28.7 to 40.8 kPa. The coatings showed negligible weight loss when stored at $100\text{ }^{\circ}\text{C}$ for 60 h, demonstrating the high thermal durability of the slippery effect. This novel strategy sheds new light on a simple fabrication method for durable icephobic surfaces.

2. Materials and Methods

2.1. Materials and Chemicals

Sylgard 184 kits were purchased from Dow Corning. It is a silicone elastomer kit and contains two chemicals, the Base (part A) and Curing Agent (part B), which are mixed in 10:1 mass ratio. Span 80 (viscosity 1000–2000 mPa·s at $20\text{ }^{\circ}\text{C}$), Tween 80 (viscous liquid), hexane (anhydrous, 95%), ethanol (99.8%) and other solvents were purchased from Sigma-Aldrich (Saint Louis, MO, USA). All chemicals were used without further purification. Ultrapure water with a resistivity higher than $15.0\text{ M}\Omega\text{ cm}$ was used in all experiments. Glass substrates were purchased from Glass Master K. Larsen & Co AS (Trondheim, Norway) and cut into $5\text{ cm} \times 5\text{ cm} \times 2\text{ mm}$.

2.2. Preparation of Hybrid Precursors

First, a silicone base and a curing agent of Sylgard 184 silicone elastomer with a weight ratio of 10:1 were mixed and stirred vigorously for 10 min, and then degassed for 30 min. Span 80 and Tween 80 with a weight ratio of 4:1 were mixed in the ultrasonic bath for 5 min, thus enabling the formation of hybrid surfactant. The PDMS component and the hybrid surfactant with different weight ratios 10%–40% were mixed, stirred vigorously for 10 min, and degassed for 30 min to remove air bubbles.

2.3. Preparation of Icephobic SLIPS Coatings

The SLIPS coatings were prepared by the following procedures. A certain weight of hybrid precursor was drip-coated on the Petri dishes and then cured at 65 °C for 4 h. The thickness of all the samples were controlled to ca. 2 mm. The four obtained coatings were marked as 10%, 20%, 30% and 40% samples based on the weight ratio of surfactant to the precursors. The pristine PDMS was also prepared for comparison. To observe the structure of the SLIPS coatings, the lubricants were removed for convenience. In detail, the SLIPS coatings were soaked in the mixture of water and ethanol (the volume ratio 1:1) for 6 h at 65 °C three times in order to remove the lubricant.

2.4. Characterization

The surface morphology of the coatings was revealed by the Scanning Electron Microscopy (FEI SEM APREO, Waltham, MA, USA), Atomic Force Microscopy (AFM, Veeco Metrology, Plainview, NY, USA) and optical microscopy (Carl Zeiss, Oberkochen, Germany). Before testing, the samples were all cleaned with dry paper to remove the superficial lubricant. All samples were sputter-coated with a 10 nm platinum/palladium layer before the SEM images. The surface morphology of the coatings was recorded by using AFM PeakForce Quantitative NanoMechanics and tapping mode. The in situ observation of the lubricating releasing process of the sample was conducted on the optical microscope (Zeiss AxoScope A1 for Reflected light BF-DIC/POL). The sample was wiped with lens paper several times and then placed on the stage of the microscope for observation of the surface morphology. The elastic modulus was measured by Quasi-static nanoindentation tests conducted in a TriboIndenter[®] 950 (Hysitron Inc., Billerica, MA, USA) using a cylindrical diamond flat punch with $53.70 \pm 0.06 \mu\text{m}$ in diameter. The samples were loaded to the maximum load (P_{max}) in 5 s and then held in the P_{max} for 10 s, followed by unloading in 5 s. The P_{max} for each sample was 10 μN . The static water contact angle was measured on a Drop Shape Analyzer (DSA100, KRÜSS, Hamburg, Germany). A measure of 5 μL of deionized water was dropped on the surfaces of the samples and the water contact angle was recorded as a function of time. The ice adhesion strength was measured by a universal mechanical tester (Instron Model 5944) equipped with a homemade cooling chamber, as described in previous reports [16,19]. A polypropylene tube with a 1 mm thick wall and 15.3 mm inner diameter was placed onto the coatings acting as an ice mold, and then 5 mL deionized water was syringed into the tube. The sample was transferred into a freezer at $-18 \text{ }^\circ\text{C}$ for more than 3 h to ensure complete freezing. Before the test, the samples were placed into the cooling chamber and stabilized at $-18 \text{ }^\circ\text{C}$ for 5 min. During the ice adhesion tests, a force probe with a 5 mm diameter propelled the tube-encased ice columns under a velocity of 0.01 mm s^{-1} , with the probe aligned close to the tested coating surface (less than 2 mm) to minimize the torque on the ice cylinder. The loading curves were recorded, and the peak value of the shear force was divided by the ice contact area on the coating surface to obtain the ice adhesion strength. In the icing/deicing cyclic tests, the same procedure as the described ice adhesion test was applied for each cycle, and the water with the tube was always placed to the same position on the sample surface immediately after one cyclic ice adhesion test. Thermal durability of the coatings was evaluated by keeping it in the oven at 100 °C for 60 h, in which the optical images and weight of the coatings were recorded before and after tests for comparison.

3. Results and Discussion

3.1. Morphology and Structure

The skins of some animals (e.g., frog) have epidermal glands with lubricant (mucus) in them (Figure S1). Figure 1b reveals the working mechanism of such skins. When the surface lubricating layer of the skin is depleted, the glands secrete mucus and repair the lubricating layer. Inspired by skins with epidermal glands, the coatings with lubricant capsules are designed and fabricated, and are marked as a 0%–40% sample corresponding to the weight ratio of lubricant to the total mass of coatings. The schematic for fabricating the SLIPS is shown in Figure S2. In contrast to the previous SLIPS,

which was done by first fabricating a porous structure and then infusing the lubricant, the current strategy directly mixes the lubricant and matrix precursors. The micellar emulsion formed in the Sylgard 184 precursor after stirring and the micelle acted as the lubricant capsules, as the lubricant consists of amphiphilic surfactant. The mixture was deposited on the substrate and then cured for further characterization. The morphology and structure of the coatings with gland-like storage and release functions are revealed by the characteristic 30% sample. The top-view and cross-sectional SEM images (Figure 1c,d) show that the surface of the coating has no obvious holes or gaps, and lubricant capsules with an average width of $ca. 1.2 \pm 0.3 \mu\text{m}$ are dispersed in the inner structure of the coating. If the lubricant is removed, the pores with an average width of $ca. 579 \pm 145 \text{ nm}$ are well dispersed in the inner structure of the coating (Figure 1e and Figure S3), which is derived from the removal of the lubricant. The AFM height images (Figure 2a–e) and corresponding phase images (Figure 2f–j) further reveal that the surfaces are flat and that the lubricant exists on the surface of the SLIPS samples (Figure 2). As shown in Figure 2a–e, in contrast to the pristine PDMS with a smooth surface without anything (Figure 2a), the liquid droplets on the surfaces of the 10%–40% samples can be seen as white parts (red arrows) on the height AFM images (Figure 2b–e) and as protrusions on the phase AFM images at the same position (Figure 2g–j). Furthermore, comparing the AFM phase and height images (e.g., circular part in Figure 2d,i) reveals that the surfaces as a whole have similar viscoelasticity, indicating that the lubricant exists over all the surfaces of coatings.

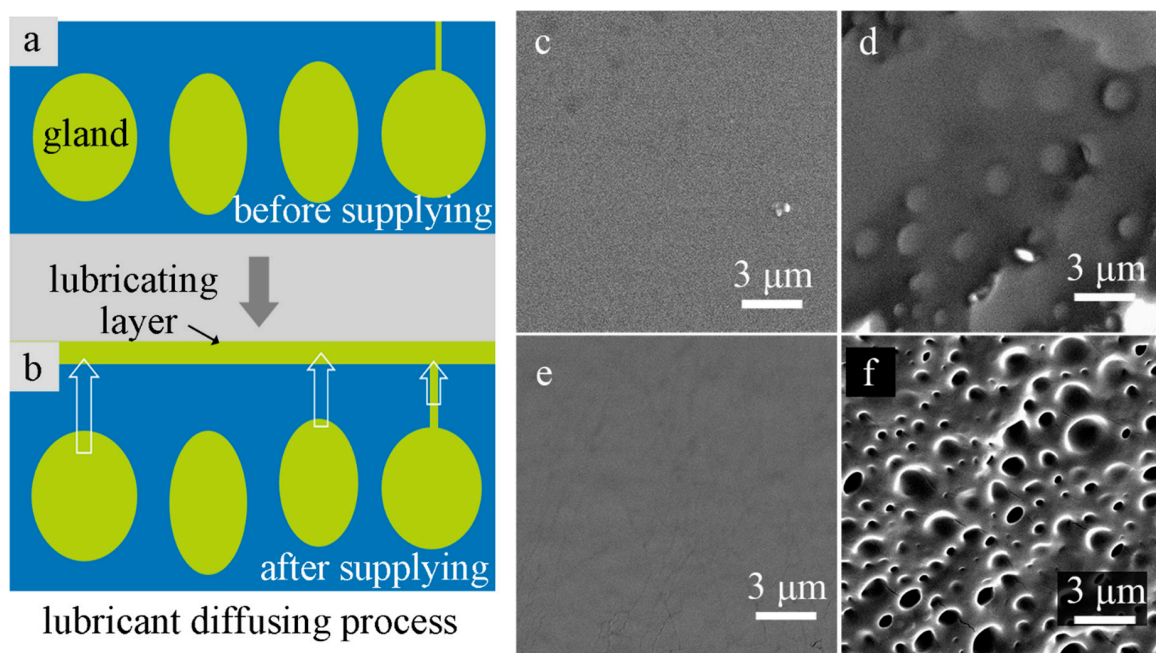


Figure 1. (a,b) Schematic of lubricant diffusing process. Top-view (c) and cross-sectional (d) SEM images of the 30% sample, respectively. Top-view (e) and cross-sectional (f) SEM images of the 30% sample after surfactant capsules being removed, respectively.

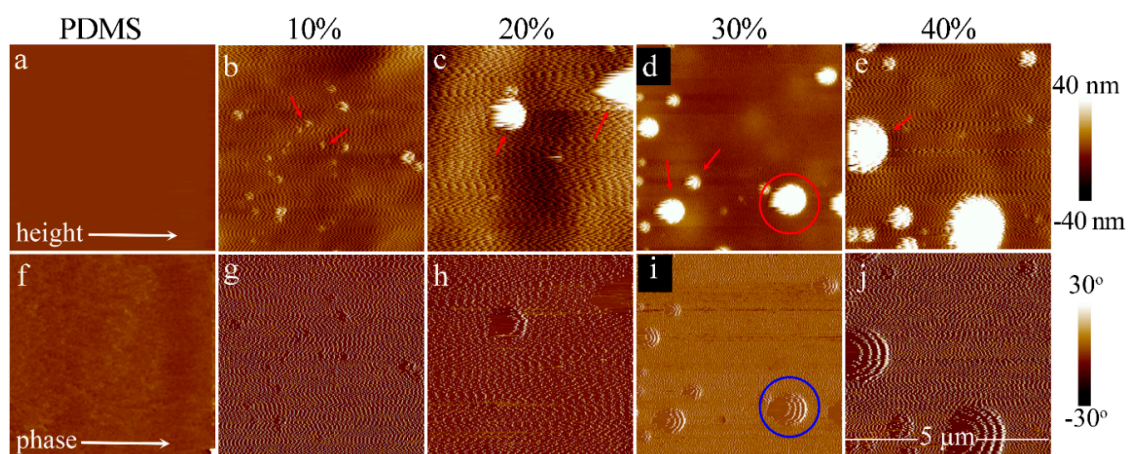


Figure 2. AFM (a–e) height and corresponding (f–j) phase images of pristine polydimethylsiloxane (PDMS), 10%, 20%, 30% and 40% coatings, respectively. The arrows and the circular parts indicate the white bulge of the coatings. The scale bar in (j) applies for the AFM images (a–j).

3.2. Chemical Composition

The variable weight ratio of the hybrid surfactant and PDMS components of the 10%–40% samples was confirmed and characterized by attenuated total reflection infrared spectroscopy (ATR-IR; Figure 3). The ATR-IR spectra of the hybrid surfactant and PDMS were also shown separately for comparison. In detail, the infrared spectra (IR) of the 10%–40% samples with variable content of surfactant are distinguished by a characteristic absorption at about 1736 cm^{-1} (dotted ellipse in Figure 3a), denoted as the ester stretch of surfactant (the chemical formula are shown in Figure S4). In contrast to no observed peak for PDMS at about 1736 cm^{-1} , the intensity of the peaks for the 10%–40% coatings progressively heightens, derived from the increasing surfactant (lubricant) content. The existence of groups from the PDMS matrix is identified at wavenumbers of 1258 cm^{-1} (CH_3 symmetric bending in Si-CH_3), 1063 cm^{-1} and 1014 cm^{-1} (Si-O-Si) and at 792 cm^{-1} (CH_3 rocking in Si-CH_3) (Figure 3b and Figure S4).

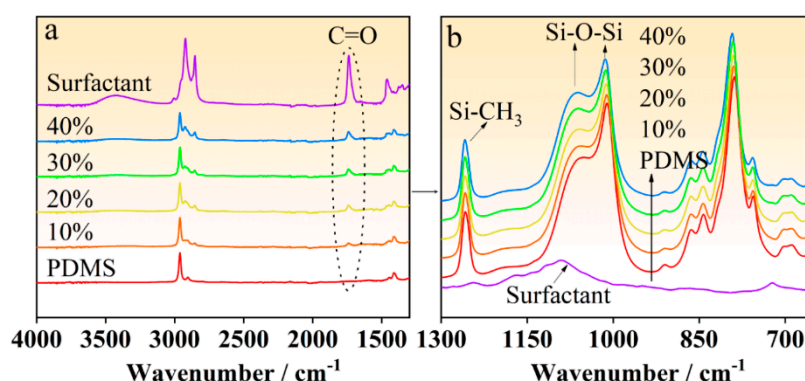


Figure 3. (a,b) Attenuated total reflection infrared spectroscopy (ATR-IR) spectra of 10%–40% samples in contrast to pristine PDMS and hybrid surfactant.

3.3. Self-Repairing Property

The self-repairing property of the SLIPS coatings was revealed by in situ observation of lubricant self-releasing behavior once the lubricant on the surface was removed. Before observing, the surface of the prepared 30% coating had plenty of lubricants (Figure S5). Then the surface was wiped with the lens paper several times to remove the lubricating layer. In Figure 4a–e, the evolution of the lubricant on the surface of a 30% coating at $20\text{ }^\circ\text{C}$ is shown in the optical micrographs. The as-prepared samples were wiped with dry paper and then observed in the initial state (0 h, Figure 4a), in which the

majority of the lubricant was removed after wiping. Compared to the micrograph at 0 h (Figure 4a), the morphology of the lubricant on the surface changes from an isolated spherical structure to a chain structure with the increase of time. The size of the lubricant increases from 2.9 to 11.7 μm , and the area ratio of lubricant on the surface increases from 3.6% to 75.7% as time increases from 0 to 60 h (Figure 4f), indicating the self-repairing of the lubricating layer after wiping. The mechanism of the self-releasing behavior is ascribed to the change in the free energy of mixing (ΔG) before and after solidification of the coatings [45]. In detail, the Sylgard 184 kits and lubricant phases are miscible with each other in the precursor state, and the free energy of mixing is negative ($\Delta G < 0$) [45]. However, the cross-linking of Sylgard 184 kits results in an increase in ΔG based on the Flory–Huggins solution theory [46], which can lead to demixing (if ΔG becomes > 0). Thus, the liquid phase can spontaneously release from the surface after curing.

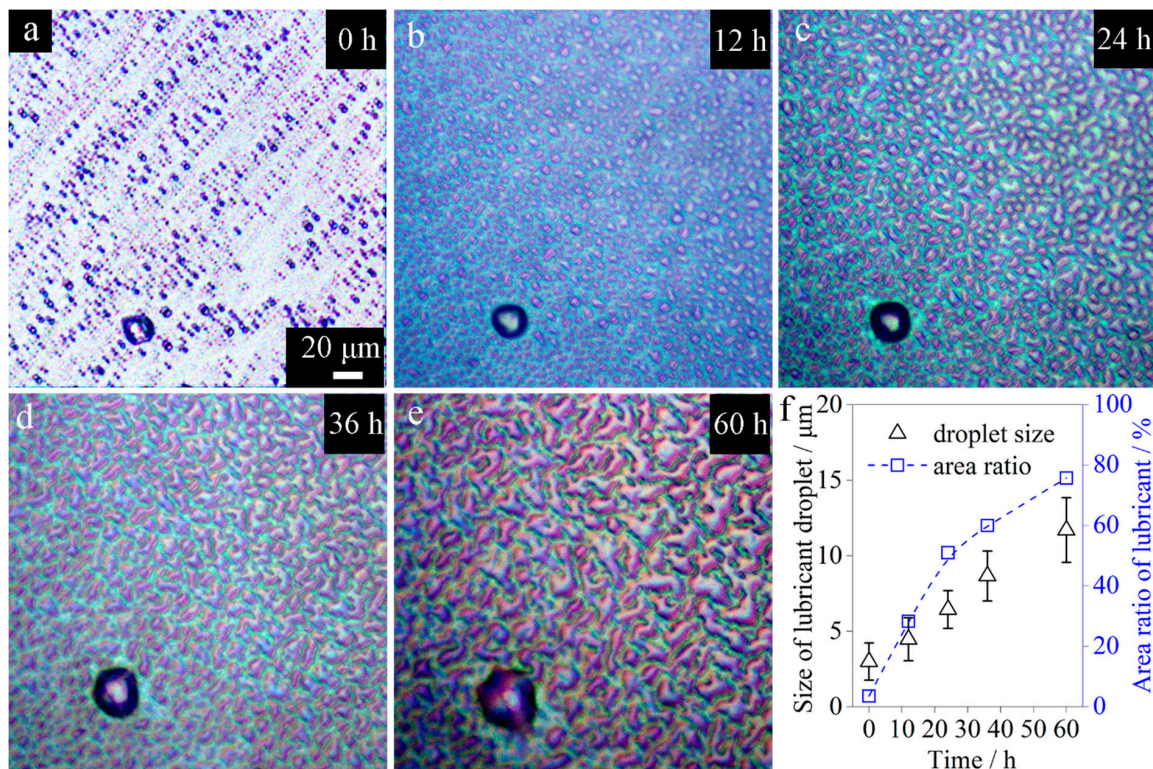


Figure 4. (a–e) In situ observation of lubricant releasing process of 30% sample at 20 °C. (f) Size of lubricant droplet and area ratio of lubricant on surfaces as a function of time.

3.4. Wettability, Mechanical Properties and Ice Adhesion Strength

According to the adhesion failure mechanism, the ice adhesion strength is related to the wettability and the elastic modulus of the materials [2]. The static water contact angles, advancing/receding contact angles and water contact angle hysteresis of the samples were investigated to reveal how the lubricant influences the wettability (Figure 5 a,b and Table S1). Figure 5a and Figure S5 show the variation of water contact angles for all tested surfaces within 80 s. While the water contact angle for PDMS is approximately stable throughout the period, that for the 10%–40% samples significantly decreases from a hydrophobic to a hydrophilic state within 80 s, due to the spread of water droplets on the lubricant-infused surfaces. Moreover, the decreasing speed of the water contact angle increases with the increase of lubricant in the coatings, implying an increase of the amount of amphiphilic lubricant (surfactant) that interacts or contacts with water droplets on the surfaces. In addition, the 10%–30% samples show similar wettability at 0 s and 80 s. This similarity may be ascribed to the identical chemical composition (surfactant with hydrophobic groups on the outside) and a sufficient modulus

for holding the water droplets. The 40% sample, however, shows a remarkably lower water contact angle than the other samples both at 0 s and 80 s, possibly due to the abundance of the surfactant on surface. Figure 5b shows the advancing/receding contact angles and contact angles hysteresis of the samples. In contrast to the advancing/receding contact angles of pristine PDMS (127.5°/68.1°), the advancing and receding contact angles of the 10%–40% coatings reduce a lot, where they change from 75.1°/15.0° to 80.2°/12.0° with the increase of lubricant. The contact angles hysteresis of PDMS and the 10%–30% coatings are close to each other (ca. 60°), while that of the 40% coating is a little lower because of its abundance of surfactant.

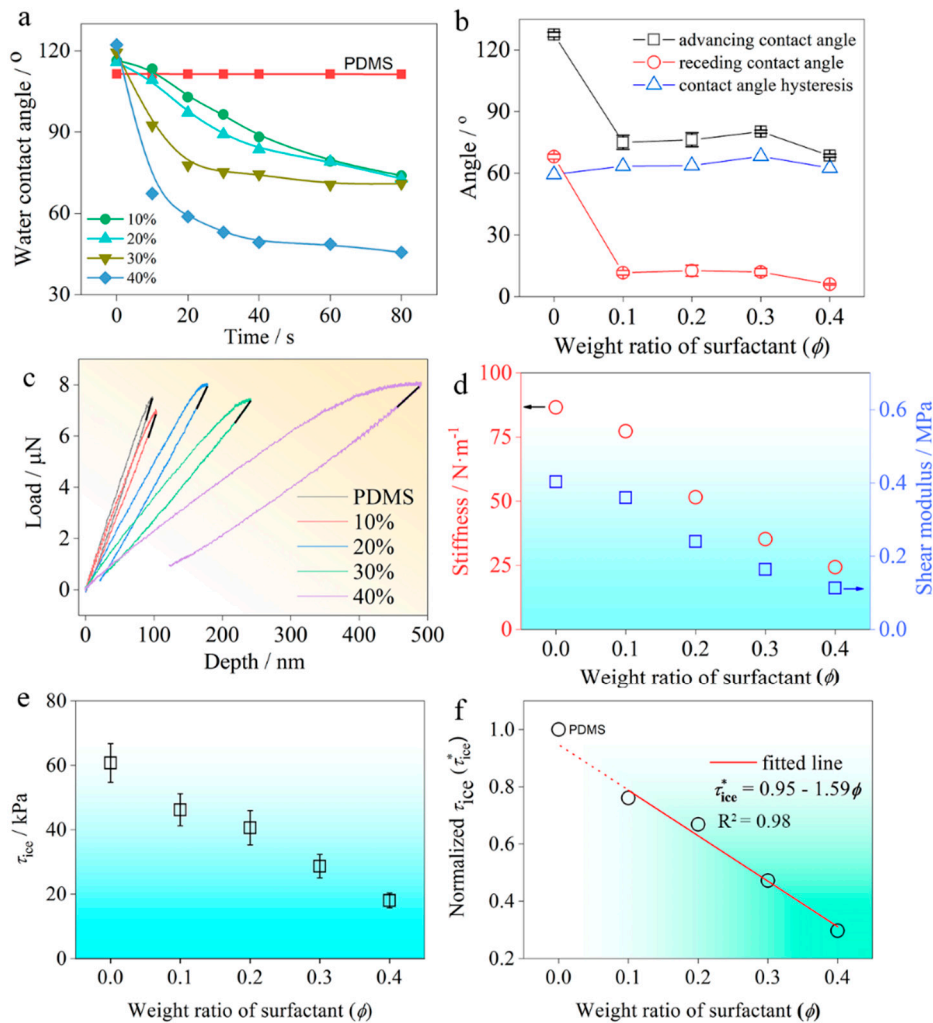


Figure 5. (a) Evolution of water contact angles for the 10%–40% samples and pristine PDMS. (b) Relationships between weight ratio of surfactant and advancing contact angles, receding contact angles and contact angle hysteresis of the samples. (c) Load-displacement curves of coatings from flat punch nanoindentation tests. Relationships between weight ratio of surfactant and (d) stiffness, shear modulus, (e) ice adhesion strength and (f) the normalized ice adhesion strength.

The ice adhesion decreases with the decrease of the modulus for elastic materials [14]. The modulus of the elastomeric coatings was investigated by the flat punch nanoindentation tests, and the resulting load-displacement curves are shown in Figure 5c. The unloading stiffness S of the SLIPS coatings is obtained by linear fitting of the initial portion of the unloading curve, as illustrated by the black fitting lines in Figure 5c. The obtained stiffness, Young's modulus and apparent shear modulus are then displayed in Figure 5d and Table 1. (The calculation processes for apparent shear modulus is shown in the supporting information). Compared to the stiffness of 86.6 N/m and the apparent

shear modulus of 0.403 MPa for pristine PDMS, both the stiffness and apparent shear modulus of the 10%–40% samples gradually decrease from 77.3 to 24.3 N/m and 0.360 to 0.113 MPa with the increased content of surfactant, respectively. In particular, the loading and unloading curves of the 10%–30% coatings display very small hysteresis, indicating excellent elastic properties. As the content of the hybrid surfactant in the PDMS framework reaches 40%, less content of PDMS leads to an obvious hysteresis behavior and to a low modulus, which is detrimental for practical applications.

Table 1. Mechanical properties of coatings prepared from varied weight ratios of hybrid surfactant.

Samples	Stiffness (N/m)	Reduced Modulus (MPa)	Young's Modulus (MPa)	Apparent Shear Modulus (MPa)
PDMS: 0%	86.6	1.613	1.210	0.403
10%	77.3	1.440	1.080	0.360
20%	51.6	0.960	0.720	0.240
30%	35.2	0.656	0.492	0.164
40%	24.3	0.453	0.340	0.113

High-performance icephobicity is one of the reported properties of SLIPS surfaces [2]. Herein, we demonstrated the possible application of our coatings for icephobicity. As shown in Figure 5e, the ice adhesion strength of the coating decreases from 46.2 to 18.0 kPa with the weight ratio of hybrid surfactant increasing from 10% to 40%, outperforming the ice adhesion strength of more than ca. 60.7 kPa for the pristine PDMS. The low ice adhesion (the lowest value: 18.0 kPa) of the coatings is favorable for practical applications, which is similar to some other SLIPS with low ice adhesion. (It should be noted that the ice adhesion strength of different studies could not be compared directly because of different testing methods) [47]. Furthermore, the relationship between ice adhesion strength and the weight ratio of the surfactant is revealed by their normalized function $\tau_{ice}^* = 0.95 - 1.59\phi$, as illustrated in Figure 5f, where the normalized ice adhesion strength of pristine PDMS sample is denoted as 1. The reduction of the ice adhesion strength is ascribed to the lubricant on the surface and the decrease of the shear modulus (Table 1 and Figure 5d) of the coatings. According to the interfacial adhesion mechanics, the ice adhesion strength is positively correlated to the interfacial energy and the shear modulus of the coatings [48]. Hence, the low ice adhesion of the surfaces is attributed to the following two parts. On one hand, the lubricant reduces the interaction between the ice and the surface. On the other hand, the introduction of lubricant leads to the reduction of the elastic modulus of the coatings, resulting in a decrease of the ice adhesion strength (Figure 5d and Table 1) based on the interfacial adhesion failure theory [14]. If the ice adhesion and mechanical properties of the coatings are considered simultaneously, the 30% coating is the optimal sample that has relatively good mechanical properties and low ice adhesion simultaneously.

3.5. Icephobic Durability

Poor mechanical durability of the liquid lubricant on surfaces is a severe problem for SLIPS materials, particularly for icephobic applications. When water or ice is removed from the surface, the liquid lubricant layer will be depleted. Consequently, the properties based on the lubricating layer degrade and even disappear. The mechanical durability of the SLIPS coatings was evaluated by the continuous icing/deicing cyclic tests. During the whole icing/deicing cyclic process, the samples were handled at $-18\text{ }^\circ\text{C}$ with no waiting in between each cycle. As shown in Figure 6a, the ice adhesion strength of the optimal sample (30% coating) increases from 28.7 kPa to 40.8 kPa after 20 icing/deicing cycles, in which the durability tested by the icing/deicing tests is much better than the SLIPS with several or even only one cycle [2,49]. Remarkably, compared to the abundant lubricant on the surfaces of the coating before the icing/deicing cycles (Figure 4), sufficient lubricant (red arrows in inset of Figure 6a) for slippery effect still exists on the coating surface after 20 icing/deicing tests (the inset in Figure 6a), demonstrating mechanical durability of the lubricating layer. The excellent durability is attributed to the self-releasing ability of the lubricating layer in addition to the properties of the material and lubricant (Figure 4). In detail, since the lubricant inside the coating structure diffuses

gradually on the coating surface, the lubricating layer on the surface is recovered when the surfactant is depleted. The self-repairing and mechanically slow loss of lubricant indicates that the coatings have high-performance mechanical durability for the icephobic property.

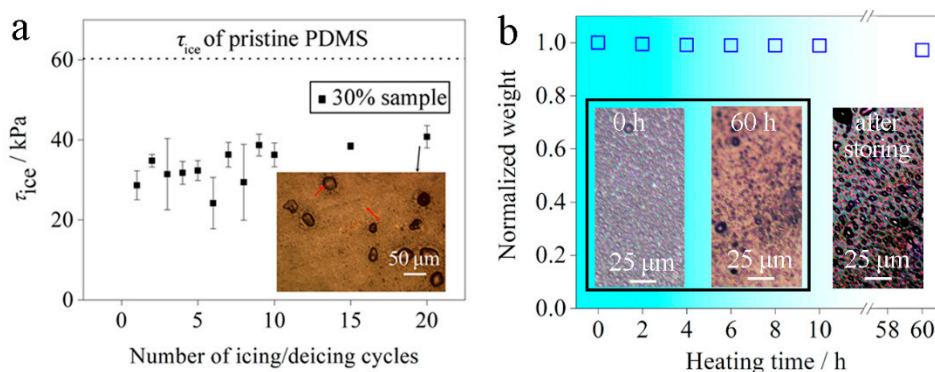


Figure 6. (a) Ice adhesion strengths of the optimized sample (30% coating) during the icing/deicing cyclic tests. The inset in (a) is the optical microscopy image of 30% coating after 20 cyclic tests. (b) Normalized weight loss of 30% sample at 100 °C with respect to time. The insets in (b) are the optical microscopy images of the coatings before and after heat-treatment and then storing for 5 days.

3.6. Thermal Durability

Liquid lubricants are prone to substantial evaporation from the opened porous structure over long periods of time in the evolving environment (e.g., changeable temperature), resulting in poor durability [50]. Herein, excellent thermal durability of the coatings was confirmed by the normalized change in weight for the 30% sample, where the initial normalized weight of the coating was donated as 1. As shown in Figure 6b, the normalized weight of the coating barely changes when the coating is kept at the temperature of 100 °C for 60 h, demonstrating good thermal durability of the coating. Meanwhile, compared to the initial surface (0 h) with abundant surfactant droplets (the left inset in Figure 6b), the surface still contains surfactant after storing for 60 h (the middle inset in Figure 6b). After the heated coating is stored in the ambient environment for 5 days, the content of the lubricant on the surface increases, indicating that the surfactant in the inner structure of the coating diffuses to the coating surface (the right inset in Figure 6b). In detail, the heat-treated coating needs ca. 5 days if the size of the lubricant droplet increase to ca. 3.1 μm (the right inset in Figure 6b), whereas it needs less than 12 h if the size of droplet increase to 3.1 μm (Figure 4f). The reduction of the repairing speed may be due to the fact that surficial lubricant in the coating evaporates during the heat treatment. As a result, much time is needed for the lubricant inside of the coating to diffuse on the surface. The high-performance thermal durability may be ascribed to the lubricant capsules packaged into the PDMS matrix, resulting in a low diffusing rate.

4. Conclusions

In summary, inspired by the epidermal glands, we developed a facile approach to durable SLIPS with lubricant storage and release functions for icephobicity. The lubricant capsules via the hybrid surfactant were formed and dispersed in the PDMS matrix, working as the gland-like structures to release lubricant. The releasing of lubricant enabled the self-repairing lubricating layer. The surface of the optimized sample still released lubricant after 20 icing/deicing test, and the ice adhesion strength increased from 28.7 kPa to 40.8 kPa, outperforming the pristine PDMS. In addition, after storing at 100 °C for 60 h, the weight loss of the coating was negligible and the lubricant still existed on the surfaces, showing a thermally durable slippery effect. The high-performance durability was then demonstrated as PDMS protecting the surfactant from evaporating in addition to an initial low evaporating rate of the lubricant. The current strategy provides a facile approach to mechanically and thermally durable SLIPS for icephobicity.

Supplementary Materials: The following are available online at <http://www.mdpi.com/2079-6412/9/10/602/s1>, Figure S1: Cross-sectional image of frog skin, Figure S2: Schematic of fabricating the coatings, Figure S3: Pore size distribution of the 30% coating after removing the surfactant, Figure S4: Chemical structural formula of Tween 80, Span 80 and PDMS, Figure S5: Optical micrograph of 30% coating before being wiped with lens paper, Figure S6: Digital images of the water contact angles of the samples at 0 and 80 s, respectively, Table S1: Properties of coatings prepared from varied weight ratio of hybrid surfactant.

Author Contributions: Conceptualization, T.L.; methodology, T.L. and Y.Z.; investigation, T.L.; writing—original draft preparation, T.L.; writing—review and editing, T.L., V.H., S.R., J.H and Z.Z.; supervision, J.H and Z.Z.; project administration, J.H and Z.Z.

Funding: This research was funded by the PETROMAKS2 Project Durable Arctic Icephobic Materials, Research Council of Norway (No. 255507), and the Norwegian Micro- and Nano-Fabrication Facility, NorFab (No. 245963).

Conflicts of Interest: The authors declare no conflict of interest.

References

1. He, Z.; Vagenes, E.T.; Delabahan, C.; He, J.; Zhang, Z. Room Temperature Characteristics of Polymer-Based Low Ice Adhesion Surfaces. *Sci. Rep.* **2017**, *7*, 42181. [[CrossRef](#)] [[PubMed](#)]
2. Kreder, M.J.; Alvarenga, J.; Kim, P.; Aizenberg, J. Design of anti-icing surfaces: Smooth, textured or slippery? *Nat. Rev. Mater.* **2016**, *1*, 15003. [[CrossRef](#)]
3. Shen, Y.Z.; Wu, X.H.; Tao, J.; Zhu, C.L.; Lai, Y.K.; Chen, Z. Icephobic materials: Fundamentals, performance evaluation, and applications. *Prog. Mater. Sci.* **2019**, *103*, 509–557. [[CrossRef](#)]
4. Rønneberg, S.; He, J.; Zhang, Z. The Need for Standards in Low Ice Adhesion Surface Research: A Critical Review. *J. Adhes. Sci. Technol.* **2019**. accepted.
5. Sojoudi, H.; Wang, M.; Boscher, N.D.; McKinley, G.H.; Gleason, K.K. Durable and scalable icephobic surfaces: Similarities and distinctions from superhydrophobic surfaces. *Soft Matter* **2016**, *12*, 1938–1963. [[CrossRef](#)] [[PubMed](#)]
6. Yin, X.Y.; Zhang, Y.; Wang, D.A.; Liu, Z.L.; Liu, Y.P.; Pei, X.W.; Yu, B.; Zhou, F. Integration of Self-Lubrication and Near-Infrared Photothermogenesis for Excellent Anti-Icing/Deicing Performance. *Adv. Funct. Mater.* **2015**, *25*, 4237–4245. [[CrossRef](#)]
7. Zhang, S.; Huang, J.; Cheng, Y.; Yang, H.; Chen, Z.; Lai, Y. Bioinspired Surfaces with Superwettability for Anti-Icing and Ice-Phobic Application: Concept, Mechanism, and Design. *Small* **2017**, *13*, 701867. [[CrossRef](#)] [[PubMed](#)]
8. Guadarrama-Cetina, J.; Mongruel, A.; González-Viñas, W.; Beysens, D. Frost formation with salt. *EPL (Europhys. Lett.)* **2015**, *110*, 56002. [[CrossRef](#)]
9. Sun, X.; Damle, V.G.; Uppal, A.; Linder, R.; Chandrashekar, S.; Mohan, A.R.; Rykaczewski, K. Inhibition of Condensation Frosting by Arrays of Hygroscopic Antifreeze Drops. *Langmuir* **2015**, *31*, 13743–13752. [[CrossRef](#)]
10. Li, T.; Zhuo, Y.; Håkonsen, V.; He, J.; Zhang, Z. Durable low ice adhesion foams modulated by submicron pores. *Ind. Eng. Chem. Res.* **2019**. [[CrossRef](#)]
11. Golovin, K.; Dhyani, A.; Thouless, M.D.; Tuteja, A. Low-interfacial toughness materials for effective large-scale deicing. *Science* **2019**, *364*, 371–375. [[CrossRef](#)] [[PubMed](#)]
12. Chatterjee, R.; Beysens, D.; Anand, S. Delaying Ice and Frost Formation Using Phase-Switching Liquids. *Adv. Mater.* **2019**, *31*, 1807812. [[CrossRef](#)] [[PubMed](#)]
13. Gao, S.; Liu, B.; Peng, J.; Zhu, K.; Zhao, Y.; Li, X.; Yuan, X. Icephobic Durability of Branched PDMS Slippage Coatings Co-Cross-Linked by Functionalized POSS. *ACS Appl. Mater. Interfaces* **2019**, *11*, 4654–4666. [[CrossRef](#)] [[PubMed](#)]
14. Golovin, K.; Kobaku, S.P.; Lee, D.H.; DiLoreto, E.T.; Mabry, J.M.; Tuteja, A. Designing durable icephobic surfaces. *Sci. Adv.* **2016**, *2*, e1501496. [[CrossRef](#)] [[PubMed](#)]
15. Lv, J.; Yao, X.; Zheng, Y.; Wang, J.; Jiang, L. Antiadhesion Organogel Materials: From Liquid to Solid. *Adv. Mater.* **2017**, *29*, 1703032. [[CrossRef](#)] [[PubMed](#)]
16. Zhuo, Y.; Håkonsen, V.; He, Z.; Xiao, S.; He, J.; Zhang, Z. Enhancing the mechanical durability of icephobic surfaces by introducing autonomous self-healing function. *ACS Appl. Mater. Interfaces* **2018**, *10*, 11972–11978. [[CrossRef](#)] [[PubMed](#)]

17. Zhang, Y.; Liu, K.; Li, K.; Gutowski, V.; Yin, Y.; Wang, J. Fabrication of Anti-Icing Surfaces by Short α -Helical Peptides. *ACS Appl. Mater. Interfaces* **2018**, *10*, 1957–1962. [[CrossRef](#)] [[PubMed](#)]
18. He, Z.; Xiao, S.; Gao, H.; He, J.; Zhang, Z. Multiscale crack initiator promoted super-low ice adhesion surfaces. *Soft Matter* **2017**, *13*, 6562–6568. [[CrossRef](#)] [[PubMed](#)]
19. He, Z.; Zhuo, Y.; He, J.; Zhang, Z. Design and preparation of sandwich-like polydimethylsiloxane (PDMS) sponges with super-low ice adhesion. *Soft Matter* **2018**, *14*, 4846–4851. [[CrossRef](#)] [[PubMed](#)]
20. Bahadur, V.; Mishchenko, L.; Hatton, B.; Taylor, J.A.; Aizenberg, J.; Krupenkin, T. Predictive model for ice formation on superhydrophobic surfaces. *Langmuir* **2011**, *27*, 14143–14150. [[CrossRef](#)]
21. Yamazaki, T.; Tenjimbayashi, M.; Manabe, K.; Moriya, T.; Nakamura, H.; Nakamura, T.; Matsubayashi, T.; Tsuge, Y.; Shiratori, S. Antifreeze Liquid-Infused Surface with High Transparency, Low Ice Adhesion Strength, and Antifrosting Properties Fabricated through a Spray Layer-by-Layer Method. *Ind. Eng. Chem. Res.* **2019**, *58*, 2225–2234. [[CrossRef](#)]
22. Cao, M.; Guo, D.; Yu, C.; Li, K.; Liu, M.; Jiang, L. Water-Repellent Properties of Superhydrophobic and Lubricant-Infused “Slippery” Surfaces: A Brief Study on the Functions and Applications. *ACS Appl. Mater. Interfaces* **2016**, *8*, 3615–3623. [[CrossRef](#)] [[PubMed](#)]
23. Wang, L.; Gong, Q.H.; Zhan, S.H.; Jiang, L.; Zheng, Y.M. Robust Anti-Icing Performance of a Flexible Superhydrophobic Surface. *Adv. Mater.* **2016**, *28*, 7729–7735. [[CrossRef](#)] [[PubMed](#)]
24. Shen, Y.Z.; Wang, G.Y.; Tao, J.; Zhu, C.L.; Liu, S.Y.; Jin, M.M.; Xie, Y.H.; Chen, Z. Anti-Icing Performance of Superhydrophobic Texture Surfaces Depending on Reference Environments. *Adv. Mater. Interfaces* **2017**, *4*, 1700836. [[CrossRef](#)]
25. Xing, Y.; Du, X.; Li, X.; Huang, H.; Li, J.; Wen, Y.; Zhang, X. Tunable dendrimer-like porous silica nanospheres: Effects of structures and stacking manners on surface wettability. *J. Alloy. Compd.* **2018**, *732*, 70–79. [[CrossRef](#)]
26. Varanasi, K.K.; Deng, T.; Smith, J.D.; Hsu, M.; Bhate, N. Frost formation and ice adhesion on superhydrophobic surfaces. *Appl. Phys. Lett.* **2010**, *97*, 234102. [[CrossRef](#)]
27. Nosonovsky, M.; Hejazi, V. Why superhydrophobic surfaces are not always icephobic. *ACS Nano* **2012**, *6*, 8488–8491. [[CrossRef](#)] [[PubMed](#)]
28. Ahn, J.; Jeon, J.; Heu, C.S.; Kim, D.R. Three-Dimensionally Programmed Slippery Wrinkles with High Stretchability for Tunable Functionality of Icephobicity and Effective Water Harvesting. *Adv. Mater. Interfaces* **2018**, *5*, 1800980. [[CrossRef](#)]
29. Niemela-Anttonen, H.; Koivuluoto, H.; Tuominen, M.; Teisala, H.; Juuti, P.; Haapanen, J.; Harra, J.; Stenroos, C.; Lahti, J.; Kuusipalo, J.; et al. Icephobicity of Slippery Liquid Infused Porous Surfaces under Multiple Freeze-Thaw and Ice Accretion-Detachment Cycles. *Adv. Mater. Interfaces* **2018**, *5*, 1800828. [[CrossRef](#)]
30. Wong, T.-S.; Kang, S.H.; Tang, S.K.Y.; Smythe, E.J.; Hatton, B.D.; Grinthal, A.; Aizenberg, J. Bioinspired self-repairing slippery surfaces with pressure-stable omniphobicity. *Nature* **2011**, *477*, 443. [[CrossRef](#)] [[PubMed](#)]
31. Smith, J.D.; Dhiman, R.; Anand, S.; Reza-Garduno, E.; Cohen, R.E.; McKinley, G.H.; Varanasi, K.K. Droplet mobility on lubricant-impregnated surfaces. *Soft Matter* **2013**, *9*, 1772–1780. [[CrossRef](#)]
32. Coady, M.J.; Wood, M.; Wallace, G.Q.; Nielsen, K.E.; Kietzig, A.M.; Lagugne-Labarthe, F.; Ragona, P.J. Icephobic behavior of UV-Cured polymer networks incorporated into slippery lubricant-infused porous surfaces: Improving SLIPS durability. *ACS Appl. Mater. Interfaces* **2018**, *10*, 2890–2896. [[CrossRef](#)] [[PubMed](#)]
33. Wu, L. Modelling and simulation of the lubricant depletion process induced by laser heating in heat-assisted magnetic recording system. *Nanotechnology* **2007**, *18*, 215702. [[CrossRef](#)]
34. Zhu, X.; Lu, J.; Li, X.; Wang, B.; Song, Y.; Miao, X.; Wang, Z.; Ren, G. Simple Way to a Slippery Lubricant Impregnated Coating with Ultrastability and Self-Replenishment Property. *Ind. Eng. Chem. Res.* **2019**, *58*, 8148–8153. [[CrossRef](#)]
35. Zheng, S.; Bellido-Aguilar, D.A.; Wu, X.; Zhan, X.; Huang, Y.; Zeng, X.; Zhang, Q.; Chen, Z. Durable Waterborne Hydrophobic Bio-Epoxy Coating with Improved Anti-Icing and Self-Cleaning Performance. *ACS Sustain. Chem. Eng.* **2019**, *7*, 641–649. [[CrossRef](#)]
36. Zhang, K.Q.; Li, X.H.; Zhao, Y.H.; Zhu, K.Y.; Li, Y.C.; Tao, C.; Yuan, X.Y. UV-curable POSS-fluorinated methacrylate diblock copolymers for icephobic coatings. *Prog. Org. Coat.* **2016**, *93*, 87–96. [[CrossRef](#)]
37. Yeong, Y.H.; Wang, C.; Wynne, K.J.; Gupta, M.C. Oil-Infused Superhydrophobic Silicone Material for Low Ice Adhesion with Long-Term Infusion Stability. *ACS Appl. Mater. Interfaces* **2016**, *8*, 32050–32059. [[CrossRef](#)]

38. Zhuo, Y.; Wang, F.; Xiao, S.; Zhang, Z.; He, J. One-Step Fabrication of Bioinspired Lubricant-Regenerable Icephobic Slippery Liquid-Infused Porous Surfaces (SLIPS). *ACS Omega* **2018**, *3*, 10139–10144. [[CrossRef](#)]
39. Zhao, H.; Sun, Q.; Deng, X.; Cui, J. Earthworm-Inspired Rough Polymer Coatings with Self-Replenishing Lubrication for Adaptive Friction-Reduction and Antifouling Surfaces. *Adv. Mater.* **2018**, *30*, e1802141. [[CrossRef](#)]
40. Federle, W.; Barnes, W.J.P.; Baumgartner, W.; Drechsler, P.; Smith, J.M. Wet but not slippery: Boundary friction in tree frog adhesive toe pads. *J. R. Soc. Interface* **2006**, *3*, 689–697. [[CrossRef](#)]
41. Cui, J.; Daniel, D.; Grinthal, A.; Lin, K.; Aizenberg, J. Dynamic polymer systems with self-regulated secretion for the control of surface properties and material healing. *Nat. Mater.* **2015**, *14*, 790. [[CrossRef](#)] [[PubMed](#)]
42. Li, J.S.; Ueda, E.; Paulssen, D.; Levkin, P.A. Slippery Lubricant-Infused Surfaces: Properties and Emerging Applications. *Adv. Funct. Mater.* **2019**, *29*, 1802317. [[CrossRef](#)]
43. Sun, X.; Damle, V.G.; Liu, S.; Rykaczewski, K. Bioinspired Stimuli-Responsive and Antifreeze-Secreting Anti-Icing Coatings. *Adv. Mater. Interfaces* **2015**, *2*, 1400479. [[CrossRef](#)]
44. Tenjimbayashi, M.; Nishioka, S.; Kobayashi, Y.; Kawase, K.; Li, J.; Abe, J.; Shiratori, S. A Lubricant-Sandwiched Coating with Long-Term Stable Anticorrosion Performance. *Langmuir* **2018**, *34*, 1386–1393. [[CrossRef](#)] [[PubMed](#)]
45. Urata, C.; Dunderdale, G.J.; England, M.W.; Hozumi, A. Self-lubricating organogels (SLUGs) with exceptional syneresis-induced anti-sticking properties against viscous emulsions and ices. *J. Mater. Chem. A* **2015**, *3*, 12626–12630. [[CrossRef](#)]
46. Flory, P.J. Thermodynamics of High Polymer Solutions. *J. Chem. Phys.* **1942**, *10*, 51–61. [[CrossRef](#)]
47. Rønneberg, S.; Laforte, C.; Volat, C.; He, J.; Zhang, Z. The effect of ice type on ice adhesion. *AIP Adv.* **2019**, *9*, 055304. [[CrossRef](#)]
48. Beemer, D.L.; Wang, W.; Kota, A.K. Durable gels with ultra-low adhesion to ice. *J. Mater. Chem. A* **2016**, *4*, 18253–18258. [[CrossRef](#)]
49. Subramanyam, S.B.; Rykaczewski, K.; Varanasi, K.K. Ice adhesion on lubricant-impregnated textured surfaces. *Langmuir* **2013**, *29*, 13414–13418. [[CrossRef](#)]
50. Zhou, W.D.; Zeng, Y.; Liu, B.; Yu, S.K.; Hua, W.; Huang, X.Y. Evaporation of Polydisperse Perfluoropolyether Lubricants in Heat-Assisted Magnetic Recording. *Appl. Phys. Express* **2011**, *4*, 095201. [[CrossRef](#)]



© 2019 by the authors. Licensee MDPI, Basel, Switzerland. This article is an open access article distributed under the terms and conditions of the Creative Commons Attribution (CC BY) license (<http://creativecommons.org/licenses/by/4.0/>).